*China Ocean Eng.*, 2020, Vol. 34, No. 4, P. 488–499
DOI: https://doi.org/10.1007/s13344-020-0044-2, ISSN 0890-5487
http://www.chinaoceanengin.cn/ E-mail: coe@nhri.cn

# A Numerical Investigation of Vortex-Induced Vibration Response and Fatigue Damage for Flexible Cylinders Under Combined Uniform and Oscillatory Flow

YUAN Yu-chao, XUE Hong-xiang*, TANG Wen-yong

State Key Laboratory of Ocean Engineering, Shanghai Jiao Tong University, Shanghai 200240, China

Received February 10, 2020; revised March 26, 2020; accepted April 22, 2020



**Abstract**

Vortex-induced vibration (VIV) for flexible cylinders under combined uniform and oscillatory flow is a challenging and practical issue in ocean engineering. In this paper, a time domain numerical model is adopted to investigate the characteristics of cross-flow VIV response and fatigue damage under different combined flow cases. Firstly, the adopted VIV model and fatigue analysis procedure are validated well against the published experimental results of a 4-m cylinder model under pure oscillatory flows. Then, forty-five combined flow cases of the same cylinder model are designed to reveal the VIV response characteristics with different non-dimensional oscillation period $T^*$ and combined ratio $r$. The combined flow cases are classified into three categories to investigate the effect of $r$ on cylinder's dynamic response, and the effect of $T^*$ is described under long and short period cases. Finally, fatigue analysis is carried out to investigate how the structural fatigue damage varies with the variations of $r$ and $T^*$. The captured characteristics of structural response and fatigue damage are explained through the VIV mechanism analysis.

**Key words:** vortex-induced vibration, fatigue damage, flexible cylinders, combined flow

**Citation:** Yuan, Y. C, Xue, H. X., Tang, W. Y., 2020. A numerical investigation of vortex-induced vibration response and fatigue damage for flexible cylinders under combined uniform and oscillatory flow. China Ocean Eng., 34(4): 488–499, doi: https://doi.org/10.1007/s13344-020-0044-2

## 1 Introduction

Vortex-induced vibration (VIV) for flexible cylinders is one of the most investigated fluid-structure interaction issues in the ocean engineering. A considerable amount of relevant researches that comprehensively introduced by Bearman (2011) and Wu et al. (2012) have been carried out to broaden the understanding of VIV. An accordant conclusion is that VIV is worthy of sufficient attention, particularly when the structural cumulative fatigue damage for flexible cylinders is concerned. In the actual marine environment, flexible cylinder is always connected to a platform at its top-end, as shown in Fig. 1. The top-end platform has to withstand the impacts of periodic wave, whose consequence is the concomitant surge motion of the platform. The riser will be forced by top-end platform to experience oscillatory motion. If the assumed ocean flow is steady, the equivalent encountered flow of the riser should be modelled as a combined steady and oscillatory flow. Compared with considering only steady flow or pure oscillatory flow, VIV for flexible cylinders under combined steady and oscillatory flow is closer to the realistic marine situations, and, much more complex inevitably.

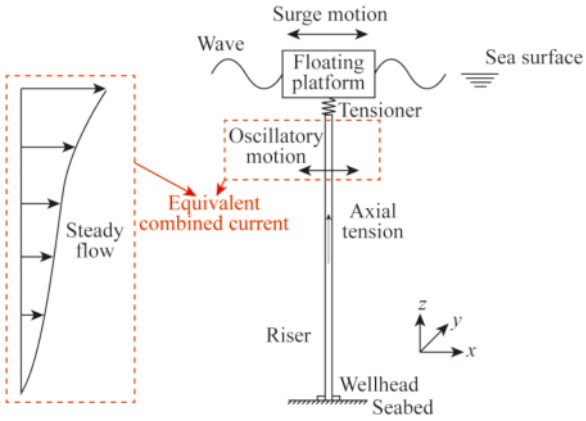


**Fig. 1.** Sketch of platform−TTR−seabed system.

The understanding of VIV under steady flow has been relatively complete, while several existing investigations concerning VIV under unsteady flow are basically performed in the view of pure oscillatory flow condition. Experiments are usually the most effective source of new insight of VIV mechanism. Over the past decades, Govardhan and Williamson (2006) and Fu et al. (2014) have sequentially carried out relevant experimental researches on

Foundation item: This paper is financially supported by the National Natural Science Foundation of China (Grant Nos. 51909163 and 51979166).
*Corresponding author. E-mail: hongxiangxue@sjtu.edu.cn

VIV of elastically mounted cylinders exposed to an oscillatory flow. Some published computational fluid dynamics (CFD) researches studied the VIV of the cylinders in oscillatory flows (Guilmineau and Queutey, 2002). Chang and Isherwood (2003) used the wake oscillator model in Orcaflex to predict an SCR's VIV in the oscillatory flow generated by top-end platform heave. Thorsen et al. (2017) developed a semi-empirical model to simulate VIV for TTR and SCR under pure oscillatory flow condition. As far as a combined steady and oscillatory flow case is concerned, Zhao et al. (2013) and Deng et al. (2014) carried out relevant CFD researches. Ulveseter et al. (2018) adopted a semi-empirical prediction tool to present the time domain simulation of a vertical riser's VIV in current and irregular waves. In general, the investigation on VIV under combined flow by different alternative methods is still in its infancy.

Force–decomposition models, which rely on the measurements of the hydrodynamic forces acting on structure from experiments, have been widely used to predict VIV for flexible cylinders (Sidarta et al., 2010; Ma et al., 2012). Force-decomposition model is adopted in this paper since it does not need extravagant computational resources or too many model controlled parameters. Firstly, the adopted numerical model and fatigue damage calculation method are validated well against the published experimental results under pure oscillatory flows in Fu et al. (2014) and Wang et al. (2015). Then, forty-five designed cases of the same cylinder are simulated to reveal how the VIV response characteristics vary with combined ratio $r$ and non-dimensional oscillation period $T^*$ under combined uniform and oscillatory flow. Finally, the fatigue damage induced by VIV under different combined flows are compared, followed by further analysis and discussions.

## 2 Numerical model

The adopted time domain force–decomposition model originates from Yuan et al. (2018). Then this paper uses it to simulate VIV under more complicated cases (i.e. combined uniform and oscillatory flows), as a consequent investigation. Cartesian coordinate system is used, where $x$-axis and $y$-axis are parallel and perpendicular with incoming flow direction, and $z$-axis is upward.

### 2.1 VIV hydrodynamic force model

Based on the force–decomposition model, cross-flow hydrodynamic force $F_{\text{hydro}}$ can be written as Eq. (1), including three force components i.e. excitation force $F_{\text{v}}$, damping force $F_{\text{d}}$ and inertia force $F_{\text{m}}$.

$$F_{\text{hydro}} = F_{\text{v}} + F_{\text{d}} + F_{\text{m}} = \frac{1}{2}C_{\text{v}}\left(\frac{A}{D}, \frac{fD}{V}, t\right)\rho_{\text{f}} D|V(t)|V(t)\cos(2\pi f t) - \frac{1}{2}c_{\text{f}}\left(\frac{A}{D}, \frac{fD}{V}, t\right)\frac{\partial y}{\partial t} - \frac{\pi}{4}C_{\text{a}}\rho_{\text{f}} D^2 \frac{\partial^2 y}{\partial t^2}, \quad (1)$$

where $C_{\text{v}}$ is the excitation force coefficient, $A$ is the cylinder's response amplitude, $D$ is the cylinder diameter, $f$ is the cylinder's response frequency, $V$ is the instantaneous combined flow velocity, $t$ is the time, $\rho_{\text{f}}$ is the fluid density, $c_{\text{f}}$ is the hydrodynamic damping coefficient, $C_{\text{a}}$ is the added mass coefficient which is assumed as a constant of 1.0 in this paper.

Hydrodynamic force coefficients $C_{\text{v}}$ and $c_{\text{f}}$ change with both response amplitude $A$ and frequency $f$, as functions of time. Fig. 2 is the contour of excitation force coefficient in phase with velocity originated from the cylinder forced vibration tests in MIT towing tank (Gopalkrishnan, 1993).

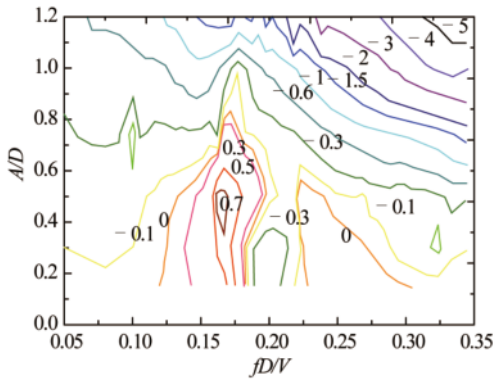


**Fig. 2.** Contour of excitation force coefficient for rigid cylinder (Gopalkrishnan, 1993).

Based on the finite element method (FEM), the cylinder is divided into a large amount of beam elements (structure segments) along its axial direction. The cylinder's displacement ($y$) and velocity ($v$) at every node and time ($t$) will be extracted at each time step to describe the real-time $A$ and $f$.

### 2.2 Lock-in judgment criterion

Lock-in is the most significant characteristic of VIV. According to Zheng (2014), this paper sets the non-dimensional frequency range of [0.125, 0.25] as the lock-in region. If the non-dimensional response frequency is located within the excitation bandwidth, lock-in occurs. The cylinder will be synchronized onto the structural natural frequency closest to $f_{\text{r}}$=0.17, where corresponds to the largest excitation force coefficient. The lock-in natural frequency is regarded as VIV dominant frequency to calculate excitation force coefficient $C_{\text{v}}$. The second-order digital control loop in Grant et al. (2000) is used to guarantee that the excitation force is in phase with the local velocity of the cylinder.

When $C_{\text{v}}$ is negative, the power is transferred from the cylinder back to fluid, and then hydrodynamic damping will act on the cylinder. If the non-dimensional response frequency is outside the excitation bandwidth, VIV dominant frequency is regarded equal to response frequency. The negative $C_{\text{v}}$ can be calculated by Fig. 2, and then the hydrodynamic damping coefficient $c_{\text{f}}$ can be calculated by Eq. (2).

$$c_{\mathrm{f}}=-\frac{C_{\mathrm{v}}\left(\frac{A}{D},\frac{fD}{V},t\right)\rho_{\mathrm{f}}V^2D}{4\pi Af}. \tag{2}$$

Outside the experimental data range, the empirical damping model proposed by Venugopal (1996) will be used.

2.3 Structural dynamic response solution

The cylinder can be considered as a flexural elastic structure satisfying the Euler-Bernoulli beam hypothesis, whose governing differential equation of cross-flow motion can be expressed as Eq. (3):

$$\left(m_{\mathrm{s}}+\frac{\pi}{4}C_{\mathrm{a}}\rho_{\mathrm{f}}D^2\right)\frac{\partial^2y}{\partial t^2}+\left[c_{\mathrm{s}}+c_{\mathrm{f}}\left(\frac{A}{D},\frac{fD}{V},t\right)\right]\frac{\partial y}{\partial t}+EI\frac{\partial^4y}{\partial z^4}-\frac{\partial}{\partial z}\left(T_{\mathrm{e}}(z,t)\frac{\partial y}{\partial z}\right)=\frac{1}{2}C_{\mathrm{v}}\left(\frac{A}{D},\frac{fD}{V},t\right)\rho_{\mathrm{f}}D|V(t)|V(t)\cos(2\pi ft), \tag{3}$$

where $m_{\mathrm{s}}$ is the mass per unit length of the cylinder; $c_{\mathrm{s}}$ is the structural damping coefficient which can be expressed as $c_{\mathrm{s}}=4\pi mf\xi$, $\xi$ being the structural damping ratio; $E$ is the elastic modulus; $I$ is the moment of inertia; $T_{\mathrm{e}}$ is the effective axial tension.

The adopted time domain numerical model is based on direct-integration dynamic analysis. Eq. (3) is solved with the Hilber-Hughes-Taylor (HHT) method, which is an implicit method that has been used successfully in classical mechanical simulations (Hilber et al., 1977). Due to its better convergence, calculation accuracy and computational efficiency, HHT method is regarded as an improved Newmark-$\beta$ method. To better demonstrate the adopted approach, the VIV analysis flow-chart within each time step is drawn in Fig. 3.

2.4 Validation against laboratory experiment

This section validates the adopted VIV model against the published test data under pure oscillatory flow of a 4-m flexible cylinder in Fu et al. (2014). The main parameters of the flexible cylinder model are listed in Table 1.

When fluid oscillates periodically in the time domain, the motion equation can be described in Eq. (4).

$$A(t)=A_{\mathrm{m}}\sin\left(\frac{2\pi}{T}t\right);\quad V(t)=A_{\mathrm{m}}\frac{2\pi}{T}\cos\left(\frac{2\pi}{T}t\right)=V_{\mathrm{m}}\cos\left(\frac{2\pi}{T}t\right), \tag{4}$$

where $A_{\mathrm{m}}$ and $V_{\mathrm{m}}$ are the maximum oscillation amplitude and oscillation velocity, $T$ is the oscillation period. Keulegan−Carpenter ($KC$) number is another key parameter to describe a certain oscillatory flow, which can be expressed as Eq. (5). Reduced velocity is one of the most important parameters of VIV under steady flows, written as $V_{\mathrm{r},n}=V/(f_nD)$, where $f_n$ is the $n$-th structural natural frequency. The maximum reduced velocity is defined as Eq. (6) for oscillatory flow cases.

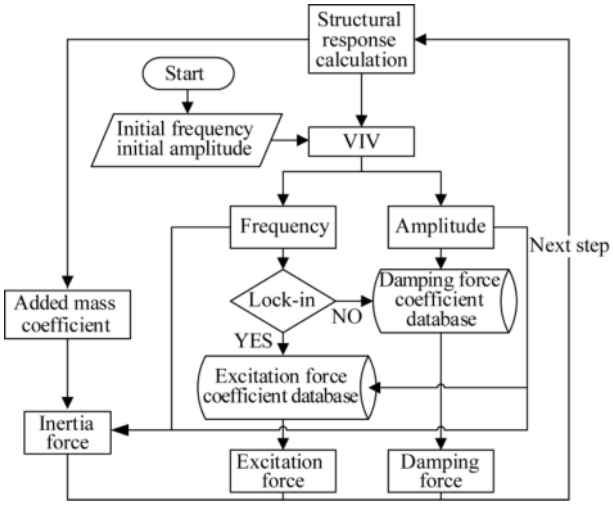


**Fig. 3.** Flow-chart of VIV analysis.

**Table 1** Parameters of the cylinder model under oscillatory flow (Fu et al., 2014)

| Parameters | Value |
|---|---|
| Length (m) | 4 |
| Diameter (m) | 0.024 |
| Bending stiffness (N·m$^2$) | 10.5 |
| Tensile stiffness (N) | $6.67\times10^5$ |
| Mass per unit length (kg/m) | 0.69 |
| Structural damping ratio | 0.015 |
| Pretension (N) | 500 |

$$KC=\frac{V_{\mathrm{m}}T}{D}=\frac{2\pi A_{\mathrm{m}}}{D}; \tag{5}$$

$$V_{\mathrm{r},1}^{\mathrm{m}}=\frac{V_{\mathrm{m}}}{f_1D}=\frac{2\pi A_{\mathrm{m}}}{Tf_1D}=\frac{KC}{Tf_1}. \tag{6}$$

A specified oscillatory flow case is characterized with a combination of $KC$ number and maximum reduced velocity $V_{\mathrm{r},1}^{\mathrm{m}}$. For the sake of conciseness, three representative cases (i.e. Case a, Case b and Case c in Table 2) are simulated to evaluate the performance of the adopted VIV model and fatigue damage calculation method. The continuous wavelet transform (CWT) technique is used to obtain the time-frequency distribution of VIV under oscillatory flows.

**Table 2** Three experimental oscillatory flow cases simulated for comparison

| Case | a | b | c |
|---|---|---|---|
| $A_{\mathrm{m}}$(m) | 0.68 | 0.12 | 0.68 |
| $T$ (s) | 10.2 | 1.8 | 16.5 |
| $KC$ | 178 | 31 | 178 |
| $V_{\mathrm{r,m}}$ | 6.5 | 6.5 | 4 |

(1) VIV response comparison

For large and small $KC$ number cases, Figs. 4 and 5 present the cross-flow VIV response comparison at mid-

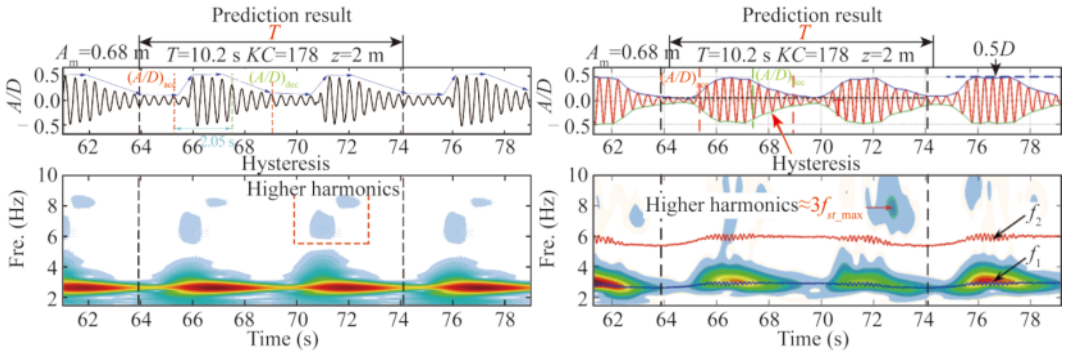


**Fig. 4.** VIV response under large *KC* number case ($V_{r,1}^{m}$=6.5, *KC*=178).

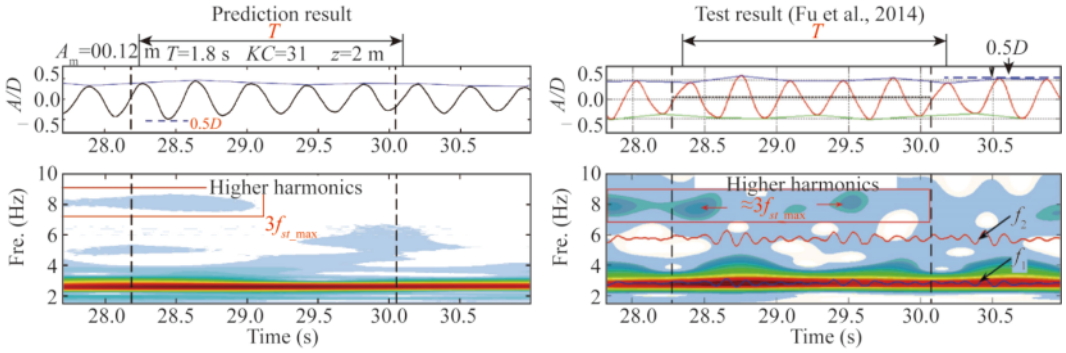


**Fig. 5.** VIV response under small *KC* number case ($V_{r,1}^{m}$=6.5, *KC*=31).

point of the cylinder (*z*=2 m) between predicted (left) and test (right) results. The top rows are displacement time histories and the bottom ones are the wavelet contour plots of strain.

For large *KC* number case i.e. Case a, intermittent and periodic VIV can be found evidently in the predicted and test displacement time histories. In general, the response amplitude would enlarge with the increase of the flow velocity and vice versa, i.e. amplitude modulation. Frequency transition can also be captured in the predicted and test wavelet contour plots. The predicted varying processes and maximum values of response amplitude as well as frequency both show good agreement with test results. From the wavelet contour plots, the higher harmonics, approximately three times the dominant frequency, can also be observed in the predicted results.

For small *KC* number case i.e. Case b, slight amplitude modulation can also be observed in VIV response displacement according to predicted and test results, but it should be distinguished from large *KC* number case. Amplitude fluctuates in time domain without evident regularity; it is more likely to be caused by unstable vibration of the cylinder, rather than the periodic pattern of flow velocity. In general, the response amplitude keeps relatively constant, and time history is quite like the sinusoidal shape under uniform flow. Both predicted and test results show that the response frequency also basically keeps unchanged with time and the comparable values are approximate.

(2) Fatigue damage comparison

Based on the laboratory experiments in Fu et al. (2014), Wang et al. (2015) carried out the corresponding structural fatigue analysis. The published results are utilized to verify the adopted fatigue damage calculation method in this paper. To calculate structural fatigue damage from predicted VIV response, there are two steps as follows: 1) Identify stress cycles from the bending stress time history based on rainflow counting approach; 2) Calculate the fatigue damage based on the Miner-Palmgren cumulative damage hypothesis with application of a certain S-N curve.

Two published cases are calculated for comparison, one is a uniform flow case with $V_{r,1}$=6.5, Wang et al. (2015) gave the predicted fatigue damage by applying VIVANA version 3.6 (Larsen et al., 2001), and the other is an oscillatory flow case with *KC*=178 and $V_{r,1}^{m}$=4 (i.e. Case c in Table 2). The test result is obtained by post-processing the measured strain signals. Accordant with Wang et al. (2015), the controlled parameters of the chosen S-N curve are $\log a$ = 15.117 and *m*=4.0.

Comparisons of VIV fatigue damage along the cylinder between predicted and published results are shown in Fig. 6. Left and right parts denote the uniform flow and oscillatory flow cases, respectively. Consistent with Wang et al. (2015), fatigue damages with and without higher harmonics for the oscillatory flow case are both calculated in the predicted results. For the uniform flow case, the predicted result gives

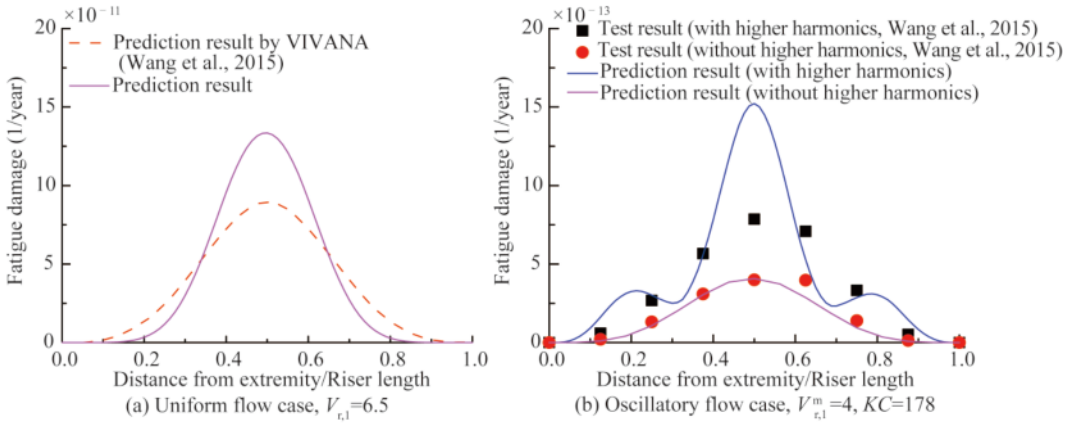


**Fig. 6.** VIV fatigue damage along the cylinder between predicted and published results.

slight underestimate near two end parts of the cylinder and overestimate at the middle than the published result from VIVANA. While overall two evaluated results have a reasonable agreement. For the oscillatory flow case, the predicted result without higher harmonics is approximately the same with test data. The predicted result with higher harmonics presents the visible third mode, corresponding to the three times harmonic component. Perhaps because the number of the measured points is limited (only 7), the third mode is not easy to be captured in the test result. Both of the predicted and test results indicate that higher harmonics increase structural fatigue damage evidently.

More detailed validating uniform flow and oscillatory flow cases could also be found in Yuan et al. (2017, 2018). Due to the lack of comparable experimental measurements, the numerical model is still difficult to be verified directly under combined flow at the present stage. Since the experimental comparison seems quantitatively good and qualitatively satisfactory under uniform flow and oscillatory flow cases, the analysis method could be speculated applicable to investigate the VIV response and fatigue damage for flexible cylinders under combined uniform and oscillatory flow.

## 3 Investigation on VIV response characteristics under combined flow

The same flexible cylinder model simulated in Section 2.4 is still utilized to investigate VIV response characteristics under combined uniform and oscillatory flow (hereafter referred to as combined flow). The instantaneous flow velocity of a combined flow can be expressed as Eq. (7).

$$V(t) = V_0 + V_{\mathrm{m}} \sin\left(\frac{2\pi}{T}t\right), \tag{7}$$

where $V_0$ is the uniform flow velocity and also the average velocity of the combined flow, $T$ and $V_{\mathrm{m}}$ are the oscillation period and maximum oscillation velocity of the oscillatory component. The combined ratio $r$ is the ratio of maximum oscillation velocity to constant velocity, $r = V_{\mathrm{m}}/V_0$.

### 3.1 Simulated cases

Designing the simulated cases systematically is an important issue for the comprehensive investigation on VIV response under combined flow. The combined flow essentially belongs to a kind of unsteady flow, and its most significant feature is time-sharing. Here defines the non-dimensional fluid parameter $V_{\mathrm{ar,n}} = V_0/(f_{\mathrm{n}}D)$ as the average reduced velocity of the combined flow. The average velocity $V_0$ mainly determines the excited fundamental frequency and modal order, with its effect on changing VIV response characteristics not as strong as the oscillatory component, and its contribution to the combined flow can be reflected by the combined ratio $r$. The non-dimensional oscillation period can be defined as $T^* = T f_{\mathrm{a,exc}}$, where $f_{\mathrm{a,exc}}$ is the excited frequency under the average velocity of the combined flow. This paper keeps $V_{\mathrm{ar},1}$ fixed at 6 (corresponding to $V_0$=0.4 m/s) for all the designed cases, i.e. VIV will stably excite the first eigenmode of the cylinder under the average velocity of the combined flow. So is $T^*$=$Tf_1$ in this study.

$KC$ number is usually used to describe an oscillatory flow. However, when an oscillatory flow is defined by its instantaneous velocity, i.e.$V(t) = V_{\mathrm{m}} \sin(2\pi t/T)$, $KC$ number is actually not an independent controlled parameter, which is determined by both oscillation period and maximum oscillation velocity ($KC = V_{\mathrm{m}}T/D$). In Fu et al. (2014) and Wang et al. (2015), when discussing the $KC$ number effect on VIV response, the maximum oscillation velocity was kept fixed. The different VIV response characteristics with the various $KC$ numbers in fact owe to the difference of the oscillation period $T$. Thus, a more independent controlled parameter $T$ is selected to design the simulated cases. Five oscillation periods from short to long (including 1.25 s, 2.5 s, 5 s, 10 s, 20 s) period cases are chosen, and they can also be deemed to cover small and large $KC$ numbers. The five chosen oscillation periods can also be expressed as $T^*$=3.4, 6.7, 13.4, 26.8 and 53.6.

The last and most important controlled parameter is the combined ratio $r$, which determines the relation between the

uniform and oscillatory components of the combined flow. Time histories of the absolute combined flow velocity with different combined ratios during each oscillation period are drawn in Fig. 7. The constant velocities corresponding to $V_{r,1}$=4, $V_{r,1}$=6, $V_{r,2}$=6, and $V_{r,3}$=6 are marked with dotted lines as well. VIV will occur evidently under steady flow situations when $4<V_{r,n}<8$ and VIV response will become the strongest at $V_{r,n}$ =6 approximately. Thus, $V_{r,1}$=4 can be defined as VIV trigger floor, below which hydrodynamic damping is dominant to weaken VIV. Beyond the trigger floor, the excitation force acts on the cylinder, and higher modes may be excited with the increase of flow velocity. $V_{r,1}$=6, $V_{r,2}$=6, and $V_{r,3}$=6 can approximately represent the excitation centers of the first, second and third eigenmodes of the cylinder.

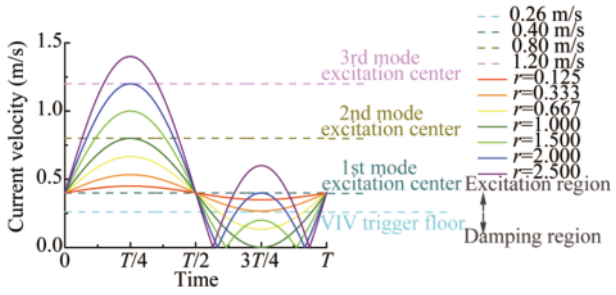


**Fig. 7.** Time histories of combined flow velocity during each oscillation period.

$r$ has significant influence on the time history of the absolute flow velocity. The combined flows can be classified into three categories according to the value of $r$. When $r \in (0, 0.333)$, flow velocity is always beyond the VIV trigger floor during the whole oscillation period, while when $r \in (0.333, 1.667)$ and $r \in (1.667, +\infty)$, flow velocity crosses over the VIV trigger floor two and four times respectively during the second half oscillation period. $(0, 0.333)$, $(0.333, 1.667)$ and $(1.667, +\infty)$ can respectively be called Ranges I, II and III. The time history shapes within Range I are generally similar, which is also true within Range III. But for Range II, the time histories may show different shapes. They can be further divided into unreversed ($r \in (0.333, 1)$), critical ($r$=1) and reversed ($r \in (1, 1.667)$) situations, depending whether the combined flow direction will reverse or not. For comprehensive consideration, all the above-mentioned types of $r$ are involved in the designed cases.

The relevant parameter selections of forty-five designed cases are listed in Table 3. $r$=0.125, 0.167 and 0.333 are on behalf of Range I. $r$=2.000 and 2.500 are within Range III. $r$=0.500 and 0.667 represent the unreversed situation, while $r$=1.000 and $r$=1.500 respectively represent the critical and reversed situations within Range II. Each column can be defined as a group, which can be utilized to discuss the combined ratio effect with a fixed $T^*$. For the non-dimensional oscillation period effect, the series of cases with Case No. equal to $p$+9$q$ ($q$=0, 1, 2, 3, 4; $p$ ranges from 1 to 9) is available, since each series has the same $r$ but different $T^*$.

### 3.2 Long period cases

The cases in Group 5 ($T^*$=53.6) are utilized to investigate the VIV response characteristics under the combined flows with long oscillation period. This section selects three representative cases i.e. $r$=0.167, 1.000 and 2.000 to reveal the respective response characteristics within Ranges I, II and III. Fig. 8 gives the structural response at the midpoint of the cylinder ($z$=2 m). The left and right parts are the time histories of the response displacement and frequency. Row 1−3 denote the case with $r$=0.167, 1.000 and 2.000, respectively. Although the time history shapes of flow velocity for the four cases within Range II may be quite different, their coincident feature is crossing over the VIV trigger floor two times. There is always a continuous time interval for the cylinder to locate below VIV trigger floor. Therefore, the response characteristics for different cases within Range II are similar.

For Range I, persistent VIV can be found although the displacement amplitude slightly fluctuates with time. The response frequency also transits within a narrow bandwidth of [2 Hz, 3 Hz], and higher harmonics can be captured near 8 Hz. Quite different from Range I, the time histories of response displacement and frequency both show that VIV within Range II is intermittent and occurs only once during each oscillation period. Note that, the maximum amplitude is approximately 0.04 m (i.e. 1.67$D$), obviously larger than that of the pure uniform flow case. From the time history of response frequency, the bandwidth of fundamental frequency becomes wider, and higher harmonics turn stronger, compared with Range I. Some amount of response energy can be captured within [5 Hz, 6 Hz], where corresponds to the second natural frequency of the cylinder. For Range III,

**Table 3** Designed combined uniform and oscillatory flow cases

| Case No. | 1−9 | 10−18 | 19−27 | 28−36 | 37−45 |
|---|---|---|---|---|---|
| $V_0$ (m/s) | 0.4 | 0.4 | 0.4 | 0.4 | 0.4 |
| $V_{ar,1}$ | 6 | 6 | 6 | 6 | 6 |
| $T$ (s) | 1.25 | 2.5 | 5 | 10 | 20 |
| $T^*$ | 3.4 | 6.7 | 13.4 | 26.8 | 53.6 |
| $V_m$ (m/s) | 0.050, 0.067, 0.133, 0.200, 0.267, 0.400, 0.600, 0.800, 1.000 | | | | |
| $r$ | 0.125, 0167, 0.333, 0.500, 0.667, 1.000, 1.500, 2.000, 2.500 | | | | |

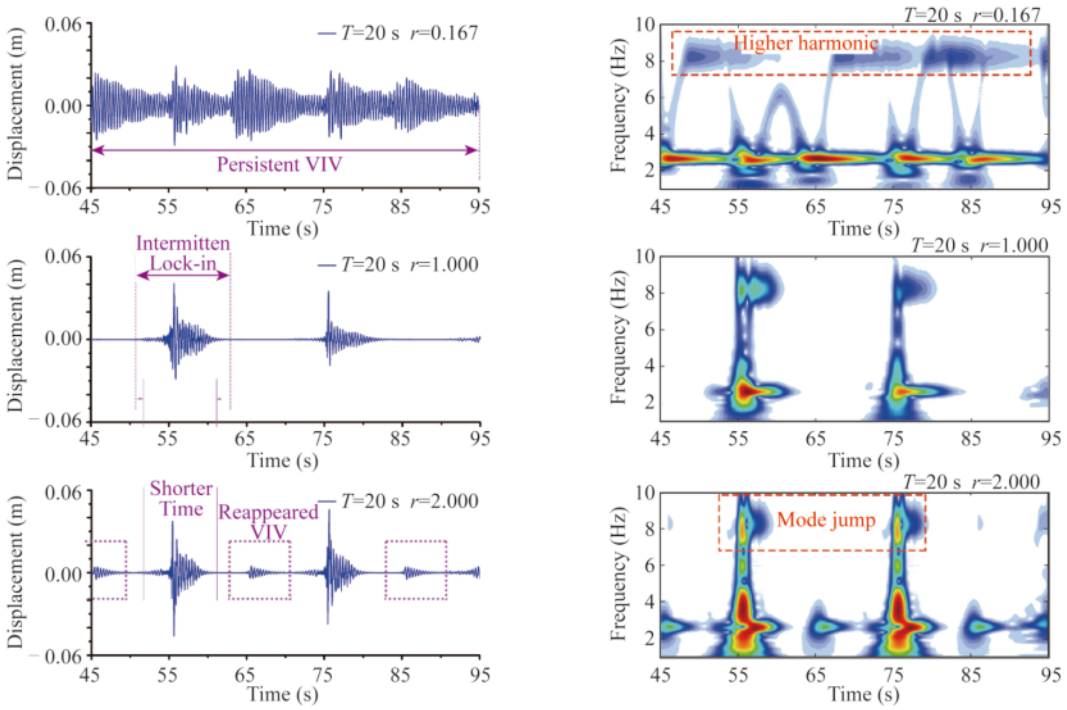


**Fig. 8.** VIV response for long period cases, Row 1: $r$=0.167; Row 2: $r$=1.000; Row 3: $r$=2.000.

the VIV response also presents some different characteristics from the former two ranges. The most significant phenomenon is the reappeared VIV. The reappeared VIV is not as strong as the adjacent ones, but it occurs stably during each second half oscillation period. Correspondingly, the time history of response frequency also shows that there are obvious response energy near $t$=45 s, 65 s and 85 s. Compared with Range II, the maximum amplitude further enlarges, and the time interval excited by VIV during the first half oscillation period becomes shorter. From the time-frequency contour plot, intensive response energy can be found near 6 Hz and 8 Hz. They should be distinguished from the higher harmonics according to their concentration level. It is reasonable to believe that the mode jumps happen, and the structural response may switch between the first three modes with time varying. In general, VIV response for long period cases has evident periodicity, and it follows a repeated regularity during each oscillation period.

### 3.3 Short period cases

Group 1 ($T^*$=3.4) is chosen to investigate the VIV response for short-period combined flow cases. Fig. 9 gives the structural response at the midpoint of the cylinder ($z$=2 m). The meanings of each sub-figure are in accordance with Fig. 8. The VIV response characteristics for short-period combined flow cases are quite different from the long-period ones. The most significant difference is that the structural response no longer presents obvious regularity or periodicity. Although amplitude modulation and frequency transition still exist, the VIV response seems not very stable.

For Range I, the time history shape of response displacement is quite similar with the uniform flow case. The response frequency basically keeps continuous and fixed at the first natural frequency, and higher harmonics are proven existent near three times the fundamental frequency. For Range II, VIV is persistent and higher modes participate in. From the time-frequency contour plot, except for the higher harmonics, some amounts of response energy appear near 6 Hz, corresponding to the second natural frequency of the cylinder. Within Range III, the time histories turn more irregular and higher-frequency response becomes more obvious. The fluctuation ranges of displacement and frequency widen. While VIV can still be deemed persistent, not as intermittent as the corresponding long period case. At $t$=63 s, the structural response jumps to the third mode evidently, but its occurrence seems not periodic during the presented 4 s (more than 3 periods). The maximum amplitude for Range I (0.018 m) is larger than that for Range II (0.015 m) but smaller than that for Range III (0.032 m).

### 3.4 General comparisons

The temporal-spatial distributions of VIV displacement for above-mentioned six representative cases are shown in Fig. 10. Left and right parts denote the long ($T^*$=53.6) and short ($T^*$=3.4) period cases, while $r$ of Rows 1−3 are 0.167, 1.000 and 2.000. Because the VIV response for long period cases has obvious periodicity, Fig. 10 just focuses on a complete oscillation period for the left side.

For long period cases, the cylinder always presents the first modal shape during a whole oscillation period when $r$=0.167. When $r$=1.000, VIV is intermittent and occurs only once during a whole oscillation period. The main excited

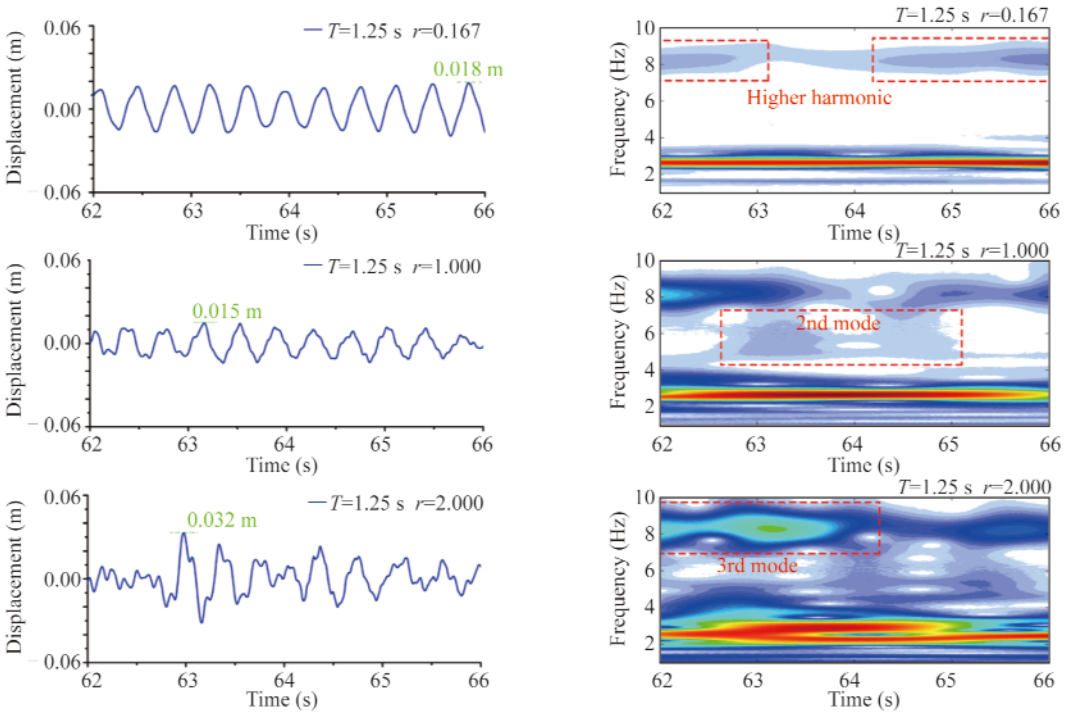


**Fig. 9.** VIV response for short period cases.

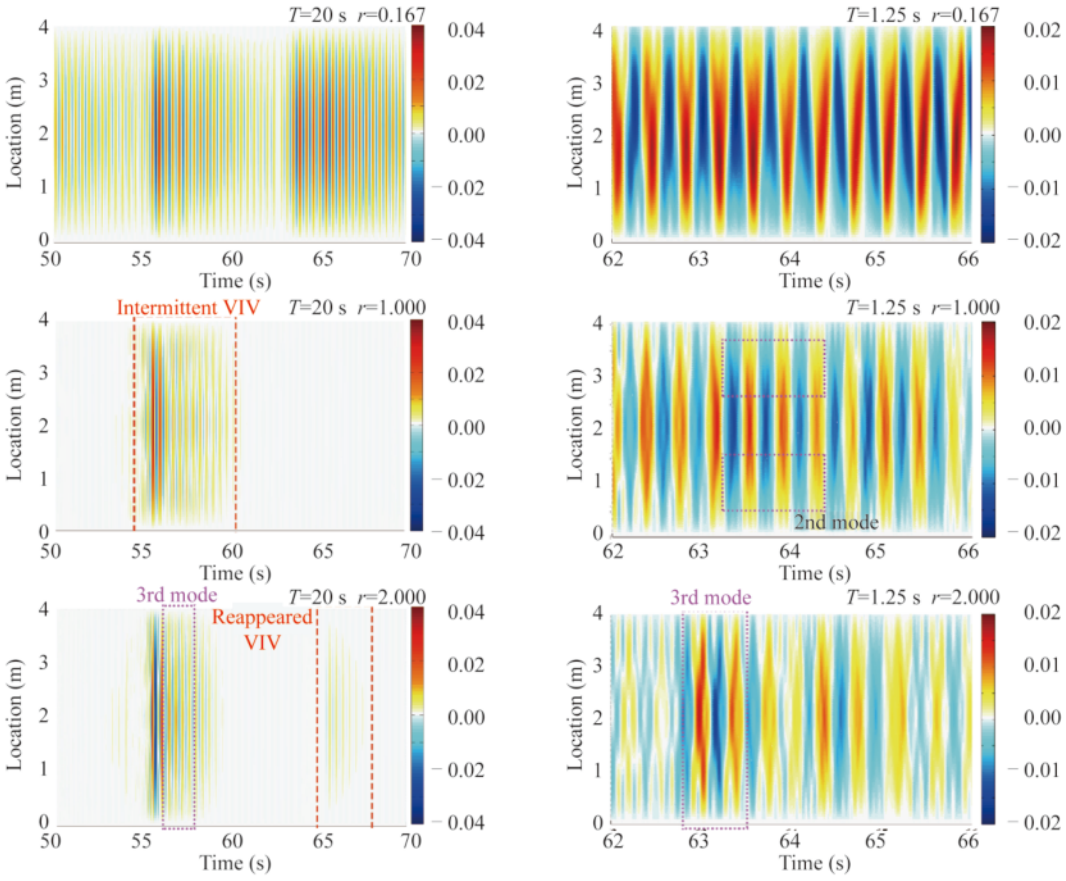


**Fig. 10.** Temporal–spatial distributions of VIV displacement under six representative cases.

mode is still the first order, but there is a tendency to present higher mode near $t$=57 s. While when $r$=2.000, intermittent VIV is captured twice. The strong and weak ones respectively appear during the first and second half oscillation peri-

od. The third modal response can be easily found within [56 s, 58 s], as marked in Fig. 10e. In fact, when $V_m$ keeps unchanged (i.e. $r$ is fixed in this paper), long-period combined flows have high $KC$ number and large oscillation amplitude. Their combined effect enables vortices to shed completely around the cylinder, so the VIV excitation force and hydrodynamic damping will affect the structural response as they do under steady flows. Associated with Fig. 7, the respective response characteristics within different ranges can be well explained with the VIV mechanism analysis.

For Range I, although the combined flow velocity reaches the extrema at $T/4$ and $3T/4$, it is always within the first mode excitation region, just slightly modulating around the excitation center $V_{r,1}$=6. The VIV response is therefore quite similar with the uniform flow case. If $r$ becomes smaller, the combined flow case can be deduced more like the uniform flow with flow velocity equal to $V_0$. Thus, Range I can be defined as the uniform-flow-like range. For Range II, the combined flow velocity will begin to decrease below VIV trigger floor within [$T/2$, $3T/4$], which means there is a quite long time interval for the cylinder to be continually dominated by hydrodynamic damping. That is why VIV is intermittent and appears once during each oscillation period. With the increase of the highest flow velocity at $T/4$ from Range I to Range II, it begins to reach the second mode excitation region, so some amounts of response energy can be found near 6 Hz in the Row 2 of Fig. 8. When it comes to the most interesting range i.e. Range III, the flow velocity gradually increases to the third mode excitation region during the first half oscillation period, so VIV response will present the third modal shape within [56 s, 58 s] and mode jumps occurs stably. While within [$T/2$, $3T/4$], the flow velocity decreases below VIV trigger floor to 0, and then inversely increases beyond the trigger floor. So the cylinder will experience excitation region to damping region twice during each oscillation period. The first excitation segment has more time and wider velocity range. Therefore, the first VIV is much stronger and excites higher modes, while the reappeared VIV relatively weakens and can only excite the first mode. Another response characteristic mentioned in Section 3.2 is that the time interval of the first VIV is obviously shorter than that of the sole VIV within Range II. Compared with $r$=1.000, the flow velocity for $r$=2.000 earlier enters damping region within [$T/2$, $3T/4$] and later leaves within [$3T/4$, $T$]. So the total time interval of the first excitation segment is shorter than that of the sole one. Within Range III, the structural response generally experiences two similar varying processes during each oscillation period. If $r$ continues to increase, the VIV response can easily be deduced more similar to the pure oscillatory flow case. Thus, Range III can be defined as the oscillatory-flow-like range. While for Range II, it can be deemed as a transition range.

For short period cases, the temporal–spatial distributions of response displacement still keep the first modal shape when $r$=0.167, but the displacement extrema appear alternately near the cylinder's two different ends. When $r$=1.000, the dynamic response along the cylinder becomes symmetric again. VIV is mainly dominated by the first mode, accompanying with the second mode sometimes being excited. While when $r$=2.000, the displacement temporal–spatial distributions are relatively disordered, and the structural response switches between different modes of the cylinder without obvious regularity. With a fixed $V_m$, short-period combined flows have small $KC$ number as well as small oscillation amplitude. Both of them make the flow field change so fast that the boundary layer separation at the rear of the cylinder will not be complete enough. When the cylinder is still located in the disturbance generated by the previous instantaneous flow, the flow velocity has changed even reversed at the next moment. In that case, the effect of fluid viscosity on structural response, which can also be deemed as the hydrodynamic damping, is not as important as steady flow situations.

For Range I, because the flow velocity is always within the first mode excitation region, the cylinder is persistently dominated by VIV excitation force. So the structural response is still quite similar with the uniform flow case. The vibration instability also makes the maximum amplitude smaller than that of the corresponding long period case. For a combined flow case within Range II and III, the excitation segment is always longer than the damping segment. The decrease of vibration amplitude needs enough time, while the time for damping to work is too short to kill the vibration so that the excitation force can dominate promptly again. Therefore the restricting effect of hydrodynamic damping on structural vibration is not as significant as steady flow situations, making VIV no longer intermittent like long period cases, but persistent in time domain. With the continuing increase of the highest flow velocity, the excited highest modal order also increases from the second to the third. However, as the flow velocity changes so fast that there is no enough time for the cylinder to form stable dynamic response, mode jumps are irregular. Compared with Range I, VIV within Range II is influenced by hydrodynamic damping remarkably, so the maximum amplitude is smaller. While for Range III, the total time interval of the two damping segments is quite short that the restricting effect is limited. And more importantly, the flow velocity can reach a much larger extremum compared with Range I, making the maximum amplitude eventually the largest among the three ranges.

## 4 Discussions on fatigue damage induced by VIV under combined flow

Structural fatigue damage is directly related to the time history of bending stress, quite dependent on the vibration mode. Especially for the combined flow cases within Ranges II and III, where mode jumps may occur, the high-

frequency response during the first half oscillation period may increase fatigue damage remarkably. While when the cylinder is dominated by hydrodynamic damping during the second half oscillation period, fatigue damage tends to be reduced. Therefore, how it varies with the controlled parameters (i.e. $r$ and $T^*$) of the combined flow is also a noteworthy issue. As mentioned in Section 2.4, higher harmonics make significant contributions to fatigue damage. However, the adopted VIV model is not yet able to predict these higher order components precisely enough. Thus, the contributions by higher harmonics are eliminated among the following fatigue analysis. The VIV response characteristics are quite different between different combined flow cases, making it necessary to investigate VIV fatigue damage under long and short period cases, respectively.

### 4.1 Long period cases

Fatigue analysis results of the nine cases in Group 5 are presented in Fig. 11 to discuss the effect of $r$ on structural fatigue damage under long period cases. For Range I i.e. $r$=0.125, 0.167 and 0.333, fatigue damage along the cylinder is clearly dominated by the first mode and decreases with the increase of $r$. $V_{r,1}$=6 is approximately the first mode excitation center. With deviating from $V_{r,1}$=6 but not reaching the second mode excitation region, VIV weakens and fatigue damage decreases.

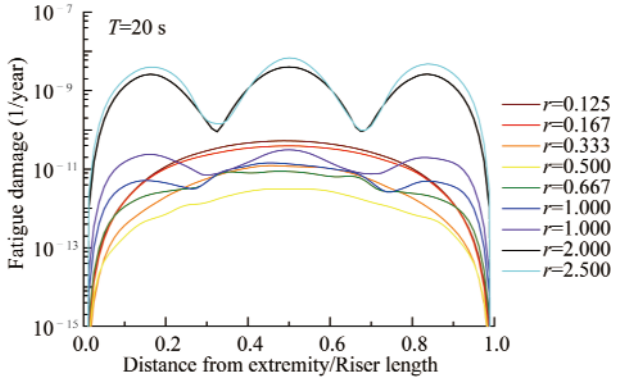


**Fig. 11.** Envelops of fatigue damage along the cylinder for long period cases ($T^*$=53.6).

For Range II, VIV still excites the first mode only and fatigue damage continues to decrease to the minimum when $r$=0.500. This is because the maximum flow velocity within the first half oscillation period is still not high enough for VIV to excite higher modes but the flow velocity has begun to enter the damping region during the second half oscillation period. As shown in Fig.7, the increase of $r$ not only increases the highest flow velocity but also lengthens the time interval of the damping segment below VIV trigger floor. The former influence will increase structural damage while the latter one tends to reduce it. The fatigue analysis results of $r$=0.667, 1.000 and 1.500 indicate that higher-frequency response appears and structural damage begins to enlarge gradually with $r$ increasing further from 0.500. It means that the increasing effect of the higher-frequency response is actually stronger than the reducing effect of hydrodynamic damping.

When $r$ comes to Range III (i.e. $r$=2.000 and 2.500), the highest flow velocity during the first half oscillation period increases continually, accompanying with stronger higher-frequency response being excited. And different from Range II, the inverse flow velocity during the second half oscillation period begins to increase beyond VIV trigger floor. The reappeared VIV captured in Fig. 10e will increase fatigue damage. Moreover, due to the existence of the second excitation segment, the previous damping segment is divided into two short ones and the total time interval of the two separated damping segments is eventually shortened. So the reducing effect of hydrodynamic damping becomes much weaker than that within Range II. The synergy combined with above three positive effects makes fatigue damage enlarger very significantly. With the increase of $r$ within Range III, the synergy turns stronger. The fatigue damage therefore tends to increase gradually with higher speed. Besides, when comparing with Range II, since the highest flow velocity is much closer to the third mode excitation center, the fatigue damage envelops for Range III shows more obvious third mode response.

### 4.2 Short period cases

The presented results of short period cases in Fig. 12 indicate that the variation trend of fatigue damage is quite similar with long period cases. For Range I, the flow velocity has not entered the damping region or higher order excitation region, making persistent VIV always excite the first mode.

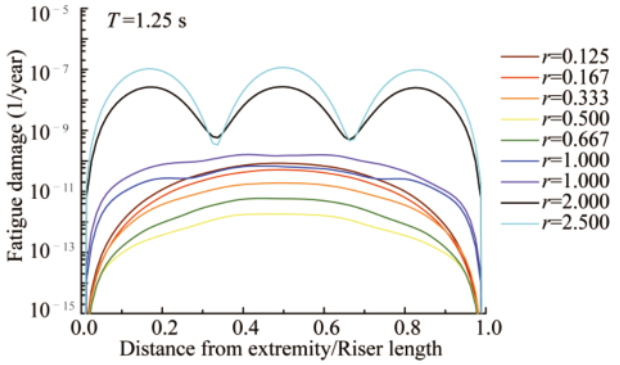


**Fig. 12.** Envelops of fatigue damage along the cylinder for short period cases ($T^*$=3.4).

When $r$ increases from 0.333 to 0.500, fatigue damage decreases to the minimum as well. However, the variation process of the envelops within Range II is a little different from long period cases, although fatigue damage still enlarges with the increase of $r$. For long period cases, the

higher-frequency response has appeared evidently since $r$=0.667. While even the result of the short period case with $r$=1.500 still mainly presents the first modal shape accompanying with less obviously higher order components. The rapidly changing flow velocity of short period cases leaves the VIV excitation force no enough time to excite higher modes stably before the cylinder goes back to the first mode excitation region, especially for the cases where the percentage of the higher order excitation segment in the whole oscillation period is low. Therefore, compared with long period cases, higher-frequency response appears later for short period cases. Even so, the fatigue damage is still dominated by the increasing effect of the higher-frequency response, thus it still enlarges with the increase of $r$.

As for Range III, larger highest flow velocity and shorter damping segments are also true, and the third mode response can be captured in Fig. 10f. So the jump from Range II to Range III leads to the significant increase of fatigue damage as well, and the envelops show the third modal shape clearly. With $r$ increasing within Range III, the increasing effect of higher-frequency response turns stronger and the reducing effect of hydrodynamic damping continues to weaken. So fatigue damage enlarges and the response features of the higher modes become more obvious.

### 4.3 Maximum fatigue damage comparisons

To discuss the effect of non-dimensional oscillation period $T^*$ on structural fatigue analysis, the maximum fatigue damage along the cylinder is collected for all simulated forty-five cases in Fig. 13. The corresponding value of the comparable uniform flow case with $V_{r,1}$=6 is marked with dotted line.

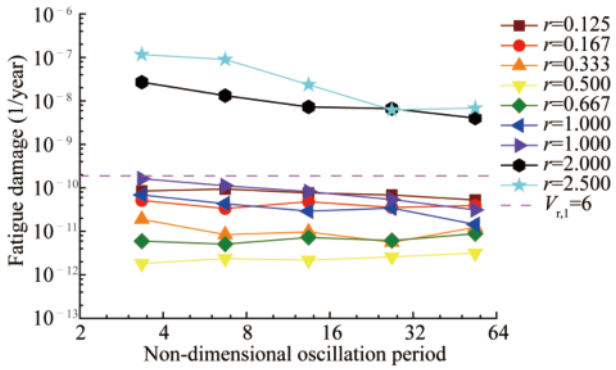


**Fig. 13.** Collection of maximum fatigue damage along the cylinder for all simulated cases.

For Range I, the flow velocity is always within the first mode excitation region, so $T^*$ influences the structural response insignificantly. When $r$ comes to 0.500 and 0.667, it is still mainly the first mode excited. Hydrodynamic damping begins to work but its influence is limited, and VIV is still persistent. While for shorter period case, the structural response turns more unstable since the varying range of flow velocity widens. Unstable single-mode response is negative to cumulate structural fatigue damage. Therefore, fatigue damage slightly increases along the $T^*$ scale.

When $r$ continues to increase within Range II, the reducing effect of hydrodynamic damping becomes stronger. Such a variation is more significant for longer period cases. This is also why there is no dynamic response during a visible time interval for long period cases while VIV under short period cases is persistent. Besides, higher-frequency response appears and makes quite important contributions to structural fatigue damage. The flow velocity of shorter period case experiences much more acceleration processes and can reach the maximum value with more times. In that case, higher-frequency response has more opportunities to be excited. Thus, for shorter period case, the reducing effect of hydrodynamic damping is weaker and the increasing effect of the higher-frequency response is much stronger, making fatigue damage decrease with the increase of $T^*$ evidently. Above analysis is also available for Range III, so the fatigue damage presents a decrease trend.

The variation of the maximum fatigue damage generally tends to be smaller with $T^*$ increasing. In fact, when the oscillation period is long enough, vortices around the cylinder can shed completely, so the VIV excitation force and hydrodynamic damping will affect the structural response as they do under steady flows. The total time intervals of various flow velocity segments (e.g. higher-frequency excitation segment, first mode excitation segment, second VIV excitation segment and damping segment et al.) are actually equal under the combined flow with different oscillation periods. So it is reasonable to deduce that the effect of $T^*$ on fatigue damage can be ignored and VIV will tend to cause stationary fatigue damage when $T^*$ is beyond a large enough value. Compared to the uniform flow case with $V_{r,1}$=6, for a combined flow case within Ranges I and II, deviation from the first mode excitation center and hydrodynamic damping below VIV trigger floor both make the fatigue damage smaller. While within Range III, the influence of hydrodynamic damping turns weaker, and more importantly, the increasing effect of the higher-frequency response has become dominant and strong enough to cause greater fatigue damage compared with the uniform flow case.

## 5 Conclusions

A time domain force-decomposition model is adopted to simulate cross-flow VIV for flexible cylinders under combined uniform and oscillatory flow. Forty-five combined flow cases with different combined ratio $r$ and non-dimensional oscillatory period $T^*$ of a 4-m cylinder model are designed to investigate the VIV response characteristics systematically. Further fatigue analysis is carried out to discuss the effects of $r$ and $T^*$on structural damage. Some conclusions are drawn as follows:

(1) The adopted VIV numerical model and fatigue ana-

lysis procedure are both validated well against the published experimental results of a 4-m cylinder model under uniform flow and oscillatory flow cases. The adopted numerical analysis approach could be speculated available in some complicated unsteady flow (e.g. combined uniform and oscillatory flow) cases.

(2) $r$ can be classified into three ranges (i.e. Ranges I, II and III). Within Range I, VIV response is similar to the uniform flow case. For longer period cases within Range II and Range III, intermittent VIV appears once and twice during each oscillation period, respectively. And the reappeared VIV within Range III is in weaker and lower order than that of the first one. For short period cases, VIV keeps persistent without obvious periodicity. When flow velocity increases beyond the first order excitation region, mode jumps occur.

(3) Within Range I, fatigue damage decreases with the increase of $r$. While within Ranges II and III, the variation trend turns inverse. When $r$ increases beyond the first order excitation region, the fatigue damage envelops gradually presents higher mode response. When $r$ jumps from Range II to Range III, fatigue damage increases significantly. Fatigue damage within Ranges I and II is less than that of the comparable uniform flow case, which will be inverse when it comes to Range III.

(4) Within Range I, the effect of $T^*$ on fatigue damage is relatively insignificant. Within Range II, if $r$ is small, fatigue damage slightly increases with the increase of $T^*$, while the variation trend turns inverse when $r$ becomes larger. Within Range III, fatigue damage decreases along the $T^*$ scale. When $T^*$ is beyond a large enough value, the effect of $T^*$ on fatigue damage can reasonably be ignored and VIV tends to cause stationary structural damage.

**References**


Bearman, P.W., 2011. Circular cylinder wakes and vortex-induced vibrations, *Journal of Fluids and Structures*, 27(5–6), 648–658.

Chang, S.H.M. and Isherwood, M., 2003. Vortex-induced vibrations of steel catenary risers and steel offloading lines due to platform heave motions, *Proceedings of the Offshore Technology Conference*, Houston, Texas, USA.

Deng, Y., Huang, W.P. and Zhao, J.L., 2014. Combined action of uniform flow and oscillating flow around marine riser at low Keulegan-Carpenter number, *Journal of Ocean University of China*, 13(3), 390–396.

Fu, S.X., Wang, J.G., Baarholm, R., Wu, J. and Larsen, C.M., 2014. Features of vortex-induced vibration in oscillatory flow, *Journal of Offshore Mechanics and Arctic Engineering*, 136(1), 011801.

Gopalkrishnan, R., 1993. *Vortex-Induced Forces on Oscillating Bluff Cylinders*, Ph.D. Thesis, Massachusetts Institute of Technology, Cambridge, MA.

Govardhan, R.N. and Williamson, C.H.K., 2006. Defining the 'modified Griffin plot' in vortex-induced vibration: Revealing the effect of Reynolds number using controlled damping, *Journal of Fluid Mechanics*, 561, 147–180.

Grant, R., Litton, R., Finn, L., Maher, J. and Lambrakos, K., 2000. Highly compliant rigid risers: Field test benchmarking a time domain VIV algorithm, *Proceedings of the Offshore Technology Conference*, Houston, Texas, USA.

Guilmineau, E. and Queutey, P., 2002. A numerical simulation of vortex shedding from an oscillating circular cylinder, *Journal of Fluids and Structures*, 16(6), 773–794.

Hilber, H.M., Hughes, T.J.R. and Taylor, R.L., 1977. Improved numerical dissipation for time integration algorithms in structural dynamics, *Earthquake Engineering and Structural Dynamics*, 5(3), 283–292.

Larsen, C.M., Vikestad, K., Rttervik, R., Passano, E. and Baarholm, G.S., 2001. *VIVANA Theory Manual*, Version 3.6, Norwegian Marine Technology Research Institute, Trondheim, Norway.

Ma, P., Qiu, W. and Spencer, D., 2012. Time-domain VIV prediction of marine risers, *Proceedings of the ASME 2012 31st International Conference on Ocean, Offshore and Arctic Engineering*, Rio de Janeiro, Brazil.

Sidarta, D.E., Finn, L.D. and Maher, J., 2010. Time domain FEA for riser VIV analysis, *Proceedings of the ASME 2010 29th International Conference on Ocean, Offshore and Arctic Engineering*, Shanghai, China.

Thorsen, M.J., Sævik, S. and Larsen, C.M., 2017. Non-linear time domain analysis of cross-flow vortex-induced vibrations, *Marine Structures*, 51, 134–151.

Ulveseter, J.V., Thorsen, M.J., Sævik, S. and Larsen, C.M., 2018. Time domain simulation of riser VIV in current and irregular waves, *Marine Structures*, 60, 241–260.

Venugopal, M., 1996. *Damping and Response Prediction of a Flexible Cylinder in A Current*, Ph.D. Thesis, Massachusetts Institute of Technology, Cambridge, MA.

Wang, J.G., Fu, S.X., Baarholm, R., Wu, J. and Larsen, C.M., 2015. Fatigue damage induced by vortex-induced vibrations in oscillatory flow, *Marine Structures*, 40, 73–91.

Wu, X.D., Ge, F. and Hong, Y.S., 2012. A review of recent studies on vortex-induced vibrations of long slender cylinders, *Journal of Fluids and Structures*, 28, 292–308.

Yuan, Y.C., Xue, H.X. and Tang, W.Y., 2017. An improved time domain coupled model of cross-flow and in-line vortex-induced vibration for flexible risers, *Ocean Engineering*, 136, 117–128.

Yuan, Y.C., Xue, H.X. and Tang, W.Y., 2018. Numerical analysis of Vortex-Induced Vibration for flexible risers under steady and oscillatory flows, *Ocean Engineering*, 148, 548–562.

Zhao, M., Kaja, K., Xiang, Y. and Yan, G.R., 2013. Vortex-induced vibration (VIV) of a circular cylinder in combined steady and oscillatory flow, *Ocean Engineering*, 73, 83–95.

Zheng, H.N., 2014. *The Influence of High Harmonic Force on Fatigue Life and Its Prediction Via Coupled Inline-Crossflow VIV Modeling*, Ph.D. Thesis, Massachusetts Institute of Technology, Cambridge, MA.